The Astrophysical Journal, 671:964–972, 2007 December 10

THE MICROWAVE PULSATIONS AND THE TEARING MODES IN THE CURRENT-CARRYING FLARE LOOPS

Baolin Tan,[1] Yihua Yan, Chengming Tan, and Yuying Liu
National Astronomical Observatories, Chinese Academy of Sciences, China
Received 2007 June 1; accepted 2007 August 9

ABSTRACT

Solar microwave observations of the X3.4 Flare/CME event observed in Chinese solar broadband radiospectrometer (SBRS/Huairou) on 2006 December 13 show a series of very short period pulsations (VSP) with the period of <1.0 s in the frequency range of 2.60–3.80 GHz. Many pulsating events have the period of only several tens of milliseconds. These pulsations are quasi-periodic, broad bandwidth, and ubiquitous during all the phases of the flare/CME event. Based on theoretical analysis of the temporal behavior of the resistive tearing mode in the electric current-carrying flare loops, we propose that microwave pulsations are a result of the modulation of the tearing-mode oscillations in the current-carrying flare loops. Our calculation of the period of the tearing-mode oscillations are in good agreement with the observations.

Subject headings: Sun: activity — Sun: flares — Sun: oscillations — Sun: radio radiation

1. INTRODUCTION

Around 2006 the Sun was in a quiet phase of the 11-year active cycle. Nevertheless, in December of this year it suddenly became furiously active. According to the *GOES* soft X-ray classification, there were four X-class flares and several M-class flares that occurred during this month, while within the past 14 months there were no X-class flares. After this month the Sun returned to its previous quiet status. We may possibly say that the Sun had an active month in its quiet phase of the 11-year cycle. Another analogous month took place in 2005 September.

In the above active month, an X3.4 flare/CME event occurred on 2006 December 13 from 02:14 UT to 02:57 UT, with the peak at 02:40 UT in AR 10930 at S06°, W21°, near the center of the solar disk. Accompanying the flare, a violent Halo coronal mass ejection (CME) and energetic particle events occurred. During this event there were many kinds of eruptive processes, e.g., bursts of X-rays, microwave bursts, etc. As for the microwave bursts at frequencies of 2.60–3.80 GHz, its right polarization was very strong, while the left polarization was very weak. There were many kinds of fine-structure phenomena: zebra patterns, spikes, fibers, diffuse continuum, and quasi-periodic pulsations. The most remarkable phenomenon was that quasi-periodic pulsations frequently occurred during all the phases of the event. Because the microwave emission region is very close to the flaring region, their periodic pulsations must carry important information about the physical conditions in flaring energy-releasing regions, and we focus on them in this work.

Microwave pulsating events have previously been observed by Young et al. (1961), Thompson & Maxwell (1962), Chiu (1970), Gotwols (1972), Elgarϕy (1986), Fu et al. (1990), and Ma et al. (2003), among others. All the available results and reports of observations show that pulsations appear widely in periods (from several minutes to subseconds) and emission frequency (from meter, decimeter, and centimeter waves). Wang & Xie (2000) classified the radio quasi-pulsating events into three kinds, according to the mean period of pulsation (P): (1) long-period pulsation (LPP), $P \sim$ tens of seconds; (2) short-period pulsation (SPP), $P \sim$ a few seconds; and (3) very short period pulsation (VSP), $P \sim$ subseconds. Aschwanden (1987, 2004) presented an extensive review of all kinds of models for the pulsating events, and classified them into three groups: (1) MHD flux tube oscillations, which modulate the radio emissivity with a standing or propagating MHD wave (slow-mode magneto-acoustic oscillation, fast kink mode, fast sausage mode); (2) periodic self-organizing systems of plasma instabilities (wave-particle, wave-wave interactions); and (3) modulation of acceleration (repetitive injection of particles into a loss-cone configuration). The third type includes nonstationary magnetic reconnection. Different kinds of pulsations may originate from different physical processes, e.g., the slow-mode magneto-acoustic oscillation may explain the pulsation with a period of 5–30 minutes, the fast kink mode may explain the pulsation with a period of 2–10 minutes, while the fast sausage mode may give an interpretation of the pulsation with $P = 1$ s to 1 minute.

There is much evidence showing the existence of the electric current system in the flaring region. The disturbances of the current system produced by some beams of fast electrons propagating in the magnetic tube will lead to dynamic processes, which in turn will stimulate radiation of the system in X-rays and microwaves, which appeared in additional to the beam-generated radio bursts. By this process , a pulsating regime can be triggered with the global sausage mode (Nakariakov et al. 2003); its period is in the range from several seconds to several tens of seconds (Khodachenko & Rucker 2005), and these pulsations belong to LPPs and SPPs.

Kliem et al. (2000) proposed another model in which the decimetric radio pulsations (0.6–2.0 GHz) are caused by quasi-periodic particle acceleration episodes that result from a highly dynamic regime of magnetic reconnection in an extended large-scale current sheet above the soft X-ray flare loop. They think that radio pulsation is a signature of dynamic magnetic reconnection, and that the reconnection is dominated by repeated formation and subsequent coalescence of magnetic islands, known as secondary tearing modes. With this model, Kliem et al. may explain the pulsations with periods of 0.5–5 s in solar flares as belonging to SPP and in part to slow VSP (with period $P =$ 100 ms $\sim$ 1 s). In particular, they may explain the global frequency of drifting pulsating structures (DPSs) as a motion of the plasmoid in the density gradient of the solar atmosphere. Here, particles are accelerated near the magnetic X-points in

[1] Datun Road A20, Chaoyang District, Beijing, 100012, China; bltan@bao.ac.cn.

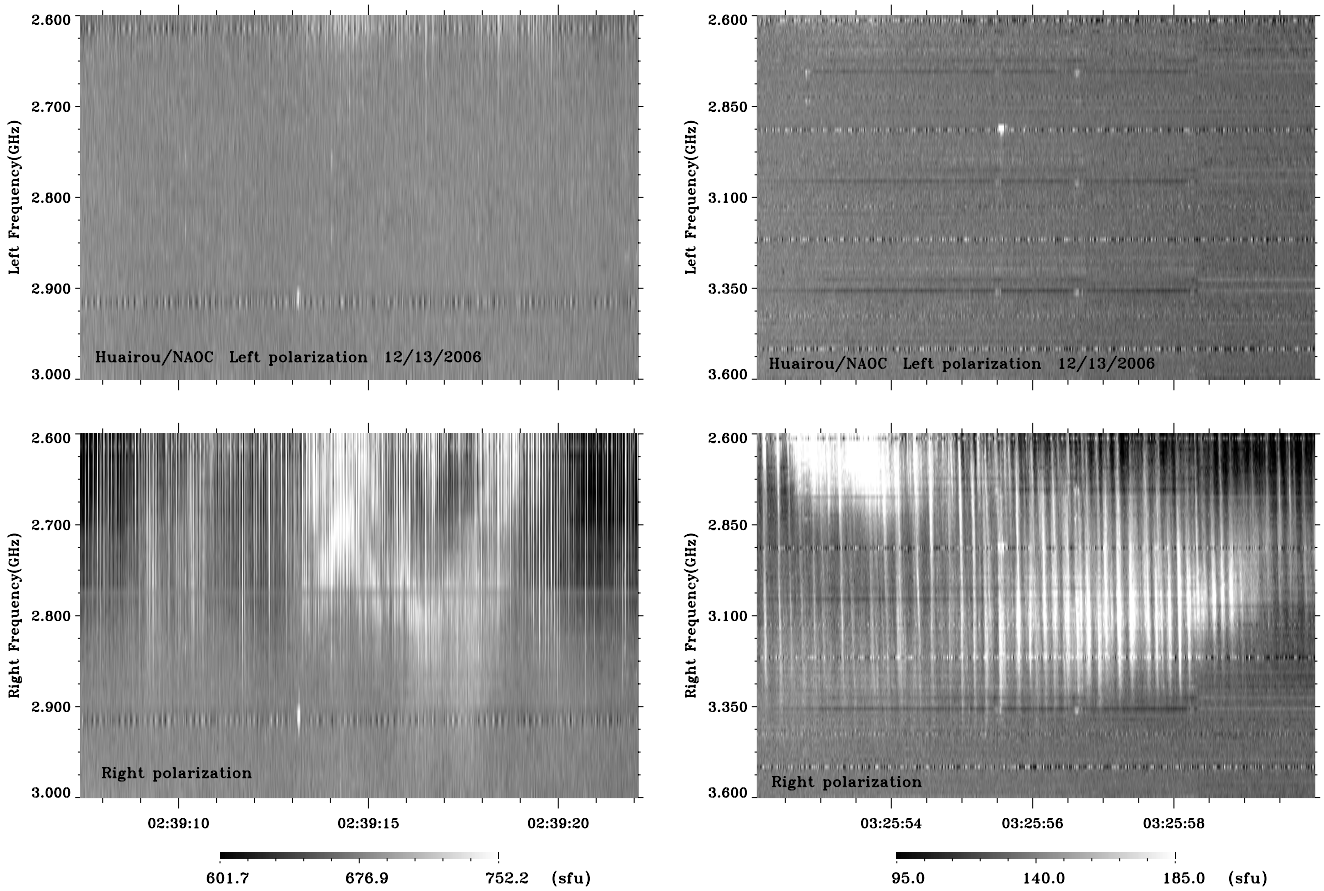

FIG. 1.—Two typical examples of solar microwave quasi-periodic pulsating events. The left panel shows an event that occurred during 02:39:08.0–02:39:22.0 UT, 2006 December 13, very close to the peak of the flare. The right panel shows an event that occurred during 03:25:52.0–03:25:59.0 UT, 2006 December 13, after the peak of the flare (SBRS/Huairou).

the DC electric field associated with magnetic reconnection. The strongest electric fields occur at the main magnetic X-points adjacent to the plasmoid, and a large fraction of the accelerated particles may only be temporarily trapped in the plasmoid; the accelerated process itself may form an anisotropic velocity distribution, which may excite the observed radio emission. Thus, the radio emission process does not necessarily require trapping in a magnetic loop. In fact, there are a series of works that explain DPSs as the radio emission generated during multiscale tearing and coalescence processes in the extended current sheet of a flare (Karlický 2004; Karlický et al. 2005). Based on particle-in-cell simulations, Karlický & Bárta (2007) found that electrons are accelerated most efficiently in the region near the X-point of the magnetic configuration at the end of the tearing process and the beginning of plasmoid coalescence. The most energetic electrons are localized along mainly the X-lines of the magnetic configuration. During these processes, plasma emission is generated and propagated. These processes may be very fast and can be used to interpret of VSPs. Zaitsev et al. (1985) proposed that the flaring plasma loop may act as resonators for MHD waves; and in particular for the fast magneto-acoustic waves, the pulsation period is $t_p \sim r/(c_A^2 + c_s^2)^{-1/2}$, which may give $P \sim 1$ s pulsations. Here, c_A and c_s denote the Alfvén speed and sound speed, respectively. As the pulsations may indicate the existence of the longitudinal electric current in the solar plasma loops, Zaitsev et al. (1998) provided another model of an LRC-circuit analog of current-carrying magnetic loop to diagnose the electric current in the solar plasma loops. In their expression, the total current in the loop is about: $I_\varphi \simeq 10^{12} P^{-1}$ (A), where P is the period of the eigen-oscillation of the LRC-circuit with the units of seconds.

However, up to now we have not had a good model for accurately interpreting fast pulsating events with a very short period of several tens of milliseconds at a frequency of microwaves. Considering the ideas of Huang (1990), Zaitsev et al. (1998), Kliem et al. (2000), Tan & Huang (2006), and Karlický & Bárta (2007) in this work, we propose a new model of the tearing-mode oscillation in current-carrying flare loops to explain the very short period pulsations. In § 2 we present the main observed features of the microwave quasi-periodic pulsations associated with the X3.4 flare/CME event; and a detailed theoretical analysis of tearing-mode oscillations in current-carrying flare loops is presented in § 3, and finally we present some conclusions and a discussions in § 4.

2. OBSERVING FEATURES OF THE MICROWAVE PULSATIONS

There is a series of good observational data in the frequency range of 2.60–3.80 GHz taken at SBRS/Huairou during the period of the above flare/CME event (Fu et al. 1995, 2004); the frequency resolution is 10 MHz, and the cadence is 8 ms. This provides us with a good opportunity to study the temporal behavior of the microwave quasi-periodic pulsations. Here, the code we utilize to analyze the observing data is from Yan et al. (2002).

First, let us track the main observing features of the microwave pulsating events. From the microwave spectrograms we may define the quasi-periodic pulsating event as consisting of a series of vertical straight bright lines, each line representing a

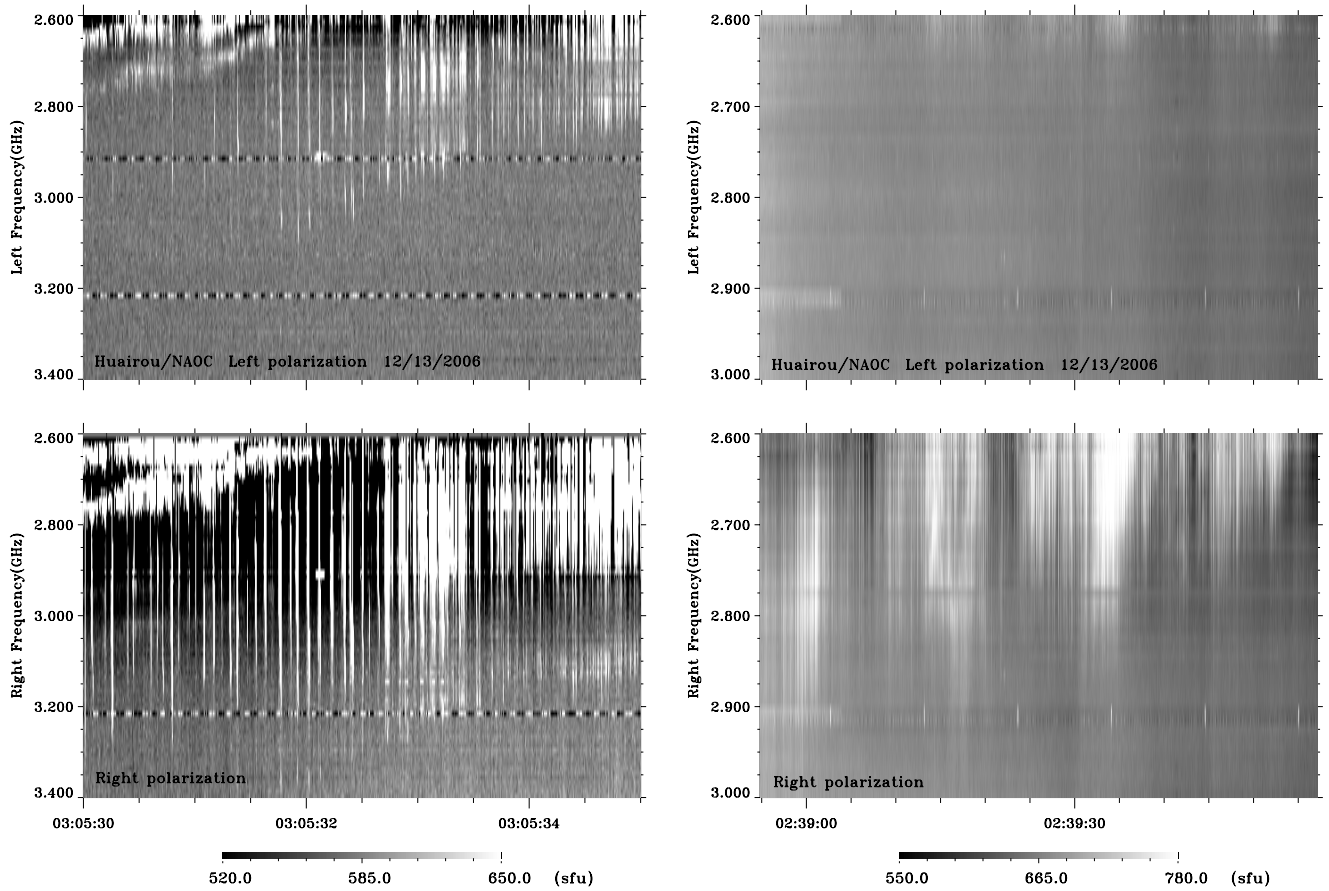

FIG. 2.—Drifting pulsating structures (DPS). The left panel shows an event that occurred during 03:05:30.0–03:05:32.7 UT, just after the peak of the flare (SBRS/Huairou). The right panel shows that there are several pulsating events that appeared one after another, which obviously have global frequency drifting from higher to lower frequency.

pulse, the space between two lines representing the period of the pulsation, and the length of the bright lines representing the emission bandwidth.

Figure 1 shows two typical examples of the pulsating events. In the left panel, the event lasts for about 13.0 s, the mean period is about 80 ms, and the central emission frequency reaches to about 2.69 GHz. From this figure the frequency drifting is not obvious, nor is the global frequency drifting rate (GFDR) or the single-pulse frequency drifting rate (SPFDR); the bright lines are almost strictly vertical to the time coordinate, and the modulation depth of the right polarizations is up to 60%. In the right panel, the pulsating event lasts for about 7.0 s, the mean period is about 165 ms, and the central emission frequency is about 3.05 GHz, and the modulation depth of the right polarizations varies from 6% to 26%. In this event it is very obvious that the bright lines are not strictly vertical to the time coordinate, the frequency drifting rate in a single pulse is $\sim$21.5 GHz s^{-1}, and the direction of the drifting is from lower to higher frequency. However, the GFDR is almost zero.

From the observation we also find that there are some pulsating events with a global frequency drifting phenomena; these phenomena are called drifting pulsating structures (DPSs; Karlický & Odstrćil 1994; Kliem et al. 2000; Kundu et al. 2001; Khan et al. 2002; Karlický et al. 2005). Figure 2 shows two examples of DPSs. The left panel shows an event during 03:05:30.0–03:05:32.7 UT, just after the peak of the flare. In this case, all the pulses as a group have an obvious slow frequency drift, with the rate GFDR ~ -86.2 MHz s^{-1}, while each of the bright lines (represent single pulses) are almost strictly vertical to the time coordinate. Near to this pulsating event, there is a zebra pattern structure (shown in the upper left corner of the figure), which may indicate that there is some relation between the pulsating event and zebra pattern structure. In the right panel of Figure 2 there are several pulsating events that appeared one right after another. In each event there is no obvious frequency drifting, but from one event to another there is an obvious slow frequency drifting, and the drifting rate is about GFDR ~ -3.36 MHz s^{-1}.

Based on a statistical analysis, we find that associated with the X3.4 flare/CME event there are about 40 or more cases of pulsating events with periods of <1.0 s. They occurred in all of the rising, peak, and postflare phases. According to the classification of Wang & Xie (2000), these pulsating events belong to the VSP (see the list in Table 1). In this table, the first column is the starting time of the pulsating event, the second column is the frequency range of the pulses, the third column is the bandwidth of the emission related to the central frequency, and the fourth column is the duration. The fifth column is the list of the periods for the pulsating events, they are identified by using two methods: (1) the statistical method, directly counting the temporal intervals between the adjacent pulse peaks during each of the pulsating events (DCT); and (2) the fast Fourier transformation with the observing data (FFT). Figure 3 shows the period results of a typical pulsating event (which occurred during 02:39:08.0–02:39:22.0 UT; see Fig. 1, *left panel*) obtained by the above two methods. The upper panel shows the statistical results at three frequencies (2.660, 2.690 , and 2.730 GHz, marked with

TABLE 1

Initial Results of Microwave Pulsating Events Associated with the X3.4 Flare (SBRS/Huairou)

Start (UT) (1)	Frequency (GHz) (2)	Bw (%) (3)	D (s) (4)	P (ms) (5)	SPFDR (GHz s^{-1}) (6)	GFDR (MHz s^{-1}) (7)	Remarks (8)
02:21:09.4	2.70–3.10	13.8	2.3	76	∞	~0	weak
02:22:07.5	2.60–2.90	>11.0	4.5	45	∞	~0	III
02:22:15.3	2.60–2.92	>11.6	3.1	58	∞	~0	weak
02:22:22.7	2.60–2.88	>10.2	5.8	40	∞	−36.2	III
02:22:46.0	2.60–3.05	>15.9	8.0	50	∞	~0	IV
02:22:58.0	2.60–3.40	26.7	6.0	35	∞	−72.7	III, ZB
02:24:25.0	2.70–3.50	25.8	4.0	61	∞	~0	IV
02:24:42.0	2.60–3.60	32.2	7.0	40	∞	−49.1	III
02:38:03	2.60–3.05	>15.9	15.0	60	∞	−24.1	ZB
02:38:46.3	2.69–2.92	8.2	2.4	35	∞	−10.2	c
02:38:57.7	2.60–2.95	>12.9	6.5	31	∞	−18.2	c
02:39:08.0	2.60–2.88	>10.2	13.0	82	∞	~0	c
02:39:24.0	2.60–2.82	>8.1	16.0	59	∞	~0	c
02:39:43.0	2.60–2.78	>6.7	13.0	76	∞	−8.2	c
02:44:05.0	2.60–2.91	>11.3	10.0	36	∞	~0	IV
02:44:25.7	2.60–2.82	>7.4	3.1	48	∞	~0	c
02:44:35.0	2.60–3.05	>16.0	10.0	59	∞	~0	IV
02:44:46.0	2.60–2.80	>7.4	4.7	45	∞	~0	IV
02:51:15.0	2.60–2.90	>10.9	5.0	59	∞	−39.3	spike
02:51:32.0	2.60–2.75	>5.6	4.8	52	∞	34.6	spike
03:01:22.0	2.60–3.05	>15.9	5.5	94	∞	−36.1	spike, ZB
03:05:15.0	2.80–3.30	16.4	8.0	62	∞	−41.1	ZB, spike
03:05:30.0	2.68–3.23	18.6	2.7	77	∞	−86.2	ZB
03:20:08.0	2.60–2.90	>10.9	14.0	70	∞	~0	c
03:23:56.0	2.62–3.14	18.0	6.0	90	22.0	−36.3	c
03:25:02.0	2.60–3.35	25.2	23.0	110	11.9	−14.2	IV
03:25:26.0	2.60–2.90	>11.0	2.20	130	20.0	~0	c
03:25:40.0	2.60–2.90	>11.0	5.0	416	8.0	~0	IV
03:25:45.5	2.60–2.90	>11.0	5.5	212	10.8	−24.0	c
03:25:52.0	2.60–3.35	25.2	12.0	165	21.5	−24.5	c
03:28:10.0	2.70–3.20	16.9	5.0	200	7.82	−24.0	weak
03:31:48.5	2.90–3.80	26.8	3.8	65	∞	~0	spike
03:34:10.0	2.60–3.80	37.5	3.8	65	∞	~0	c
03:34:40.0	2.60–3.80	37.5	5.0	55	∞	~0	c
03:35:19.0	3.15–3.80	18.7	11.0	59	∞	−13.6	spike
03:35:30.0	2.90–3.80	29.1	10.0	70	∞	~0	c
03:42:15.8	2.95–3.68	22.1	2.2	110	20.0	−13.3	weak
03:44:09.0	2.85–3.65	24.6	5.0	160	11.3	32.5	c
03:44:55.0	2.60–3.40	26.7	7.0	140	12.8	−8.9	c
03:45:10.0	2.70–3.10	13.8	5.0	156	6.83	−31.4	c
03:57:22.0	2.60–3.80	37.5	8.0	40	∞	~0	spike

Notes.—Bw is the relative bandwidth of emission, D is the duration, P is the period, SPFDR is the frequency drifting rate in a single pulse, GFDR is the averaged global frequency drifting rate, and III, IV, and ZB indicate type III burst, type IV burst, and zebra pattern structure, respectively. A "c" indicates that only pulsations occurred.

an A, B, and C, respectively) obtained by DCT. It indicates that the most prominent pulsation is with the period of about 80 ms. The lower panel shows the Fourier power spectrum curves (at the same three frequencies as above) obtained by FFT. From these curves we can see that the most prominent pulsation also has a period of about 80 ms. From the comparison of these two results we find that their results are in good agreement with each other. The sixth column of Table 1 is the frequency drifting rate in single pulses (when SPFDR $\gg$ 30 GHz s^{-1} it is marked as ∞), and the seventh column is the averaged global frequency drifting rate in the pulsating event as a whole (GFDR).

Figure 4 shows the distribution of the pulsating events during the flare at the time coordinate. The upper panel shows the microwave flux curve at a frequency of 2.840 GHz, and the lower panel shows a soft X-ray light curve (*GOES*), in addition to the temporal relationship with the soft X-ray and microwave flux. From this figure and Table 1 we find that the pulsating events associated with the X3.4 flare/CME event possess the following features:

1. The duration (D) of periodic pulsating events is in the range of 2.3–23.0 s. The right polarization is very strong (the comparisons from the upper panel to the lower panel in Figs. 1, 2, and 5 reveal this point to a certain extent).

2. The mean period (P) is 31–416 ms; they all belong to VSPs. Among them, about 75.6% are pulsating events (31 in 41 events) with the period of $P < 100$ ms; we call there fast VSPs (a subkind). The other 24.4% events with the period of $P \geq 100$ ms are called slow VSPs (another subkind). Before the peak of the flare all of the pulsating events belonged to fast VSP, and all of the slow VSP appeared after the peak of the flare.

3. The emission bandwidth (Bw) is in the range of 230–1200 MHz, and the relative bandwidth is about (8.2%–37.5%).

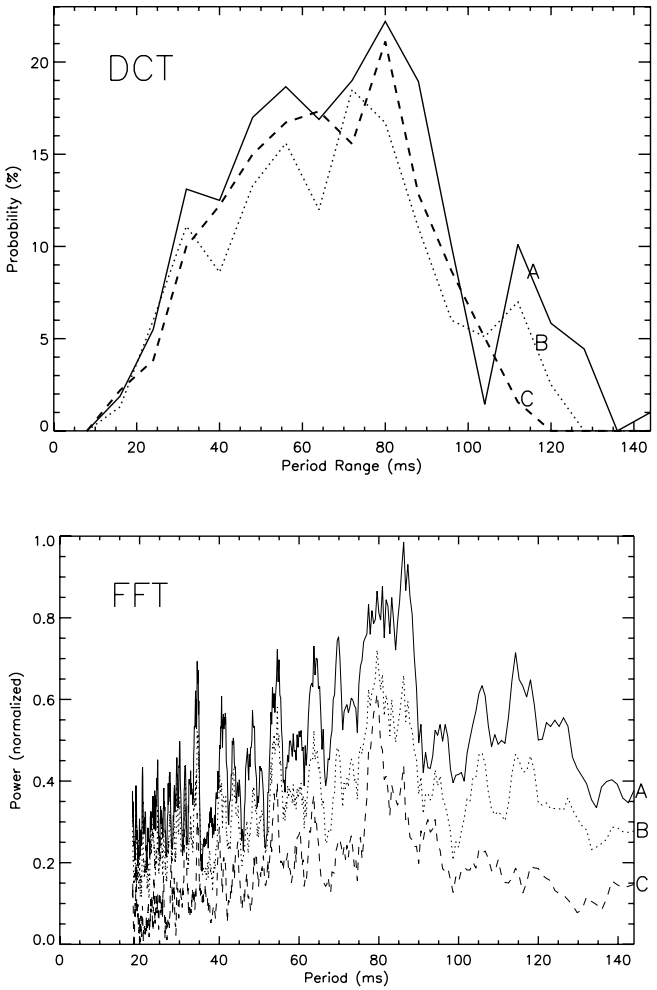

FIG. 3.—Two methods to identify the period of the pulsating event (a typical example occurred during 02:39:08–02:39:22 UT, shown in Fig. 1, *left panel*). The upper panel shows the result of the statistical method (DCT), while the lower panel is a Fourier power spectra from the fast Fourier transformation (FFT). Here the lines A, B, and C represents the results at 2.660, 2.690, and 2.730 GHz, respectively.

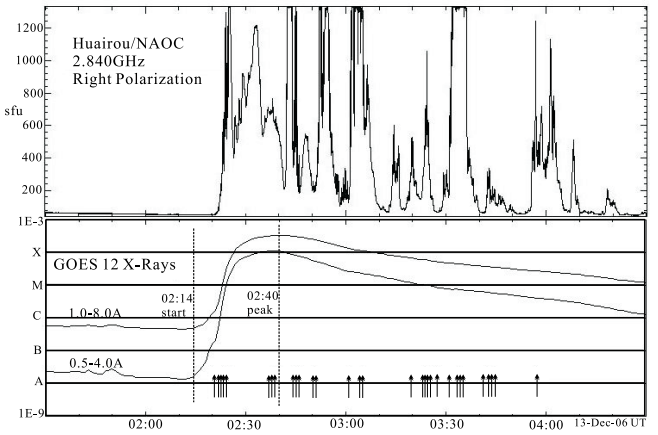

FIG. 4.—Distribution of the pulsating events during the flare/CME event with a radio flux of 2.840 GHz (*upper panel*, SBRS/Huairou) and *GOES* soft X-ray curve (*lower panel*). The arrows indicate the start time of the pulsating events at the time coordinate.

However, there are many cases in which the frequency range extended below 2.60 GHz and above 3.80 GHz; their relative bandwidths must be greater than the value marked in Table 1.

4. The frequency drifting rate in a single pulse is very large, in most cases SPFDR $\rightarrow \infty$. Only in some of the slow VSP events may we distinguish the drifting feature of a single pulse (see in Table 1) from the drifting rate (SPFDR $\sim$ 5.83–30.0 GHz s^{-1}) that is much larger than those of the type III bursts. The global frequency drifting rate of the pulsating event is in the range of -86.2 MHz s^{-1} $\sim$ 34.6 MHz s^{-1}, and most of them are negative, i.e., drift from higher to lower frequencies; only two cases drift from a lower to a higher frequency (they are all after the peak of the flare). In fact, when GFDR $\neq 0$, they belong to DPSs (Karlický & Odstrčil 1994; Kliem et al. 2000; Kundu et al. 2001; Khan et al. 2002; Karlický et al. 2005). However, for the same reason as in many cases with frequency ranges extending below 2.60 GHz and above 3.80 GHz, their GFDR, shown in Table 1, are not very accurate, being only approximations.

5. Before the peak of the flare, some of the pulsating events are accompanied with type III bursts and zebra pattern structures, while after the peak of the flare, most of the pulsating events are accompanied with spikes. The left panel of Figure 5 shows that a pulsating event is concomitant with a type III burst and a zebra pattern structure (Yan et al. 2007) during 02:22:58–02:23:07 UT, before the peak of the flare. The period of the pulsating event is about 35 ms, SPFDR $\rightarrow \infty$ and GFDR ~ -72.7 MHz s^{-1}. The bandwidth of the type III burst is more than 1.20 GHz, and its frequency drifting rate is about 2.10 GHz s^{-1} from low to high frequency, with a duration of about 1 s. The type III burst was so strong that it completely submerged the pulsations in the background. The zebra pattern consists of eight strips, and its frequency drifting rate is about -80 MHz s^{-1}. The right panel of Figure 5 presents a great multitude of spikes distributed along the vertical pulsating bright lines, during 03:57:21–03:57:29 UT, more than 1 hr after the peak of the flare, and the period of the pulsation is about 40 ms. If we scrutinize the pattern, we find that the original spikes are distributed stochastically and modulated by some pulsating factors.

3. THEORETICAL ANALYSIS

As mentioned in § 1, it is still an open question as to which pulsating mechanisms are relevant for the interpretation of the observing features, and how the proposed model works in detail, especially for the very short period pulsations (VSP). In this section, we attempt to present a new theoretical interpretation of the VSP by adopting the tearing-mode oscillation in the current-carrying flare loops.

It is well known that in current-carrying plasma systems, the tearing modes may lead to magnetic islands forming a new, geometrically more complex, equilibrium configuration (Biskamp & Welter 1980). Electrons circulating within the magnetic islands will gain energy in a classic Fermi manner as they reflect from the moving ends of the islands (Drake et al. 2006). Kliem et al. (2000) have studied the effect of the current sheet on the quasi-periodic pulsations with a period of 0.5–5 s. However, for the fast VSPs at frequencies of 2.60–3.80 GHz, the period slows down to only about several tens of milliseconds; using the above models (including the model of Zaitsev et al. 1998) we could not find a reasonable explanation for this. In fact, in the current-carrying plasma loops, the resistive tearing mode will also be naturally excited (Furth et al. 1973). Many studies have used the instability and the growth rate of tearing modes to explain the solar eruptive phenomenon (Heyvaerts et al. 1977; Spicer 1981; Hassam 1990; Tan et al. 2006), such as solar flares. However, the oscillations of the resistive tearing modes are always neglected. Huang (1990)

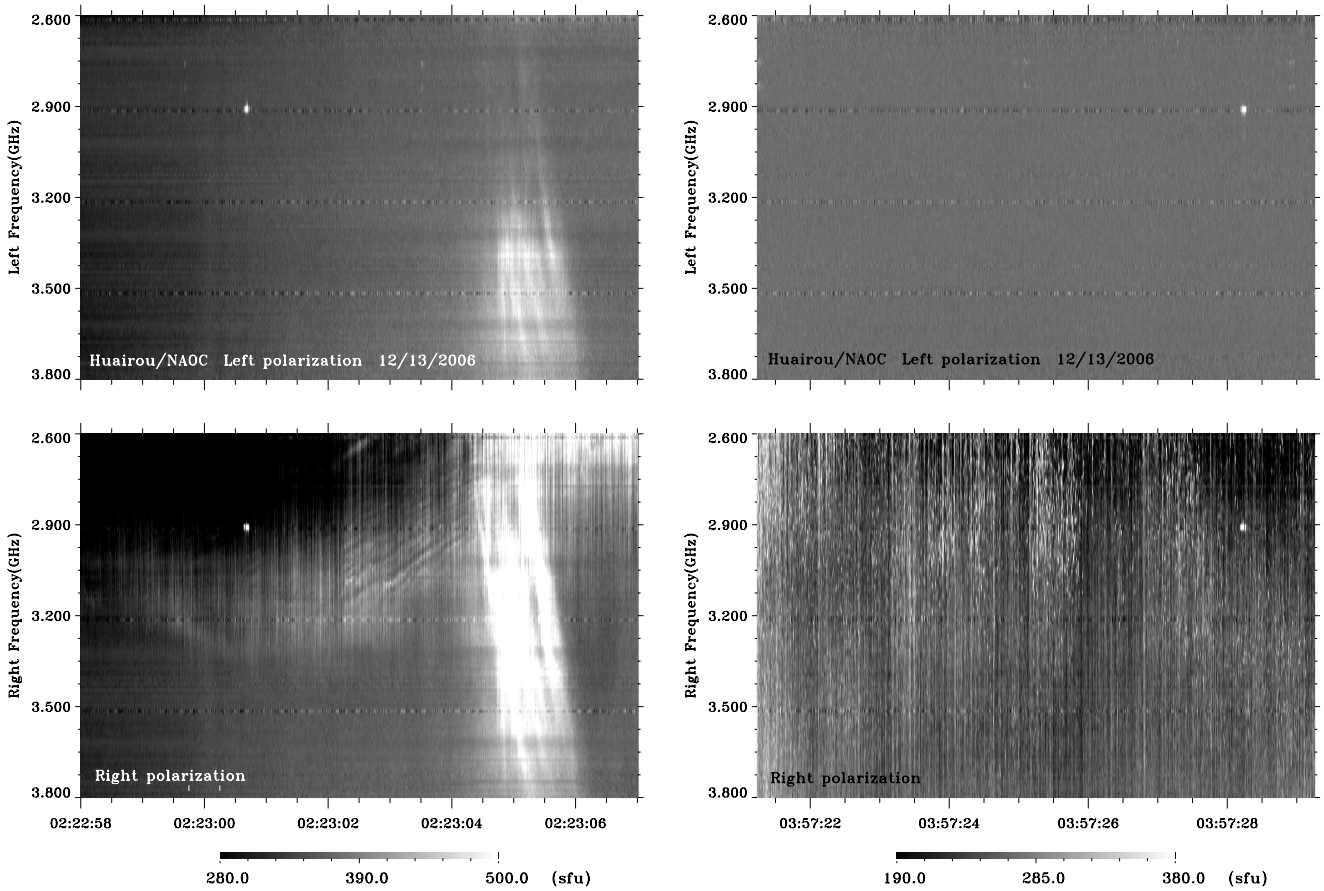

FIG. 5.—Left panel shows the relationship between the microwave periodic pulsations and the zebra patterns and type III bursts during 02:22:58–02:23:07 UT, before the peak of the X3.4 flare event. The right panel shows snowflake-like spikes distributed along the vertical lines of the solar microwave pulsations during 03:57:21–03:57:29 UT, quite a bit after the peak of the flare. (SBRS/Huairou)

applied tearing-mode oscillation in a current sheet to explain the millisecond radio spikes and got good agreement with the microwave observation; but there is no comparable discussion in works on current-carrying coronal loops, there are no comments about the oscillations of tearing modes. As the plasma density, corresponding to frequencies of 2.60–3.80 GHz, is about 10^{16}–10^{17} m^{-3}, it is much closer to the inner part of the flare loop, away from the region of the current sheet. Thus, we attempt to use the pulsations of the resistive tearing-mode oscillation in current-carrying flare loops to explain the origin of VSPs.

Differing from the regime of current sheets, in current-carrying plasma loops we describe the magnetic field in cylindrical coordinates

$$\boldsymbol{B} = B_z(r,z)\boldsymbol{e}_z + B_\theta(r,z)\boldsymbol{e}_\theta. \quad (1)$$

Based on the conditions $\nabla \cdot \boldsymbol{B} = 0$ and $\nabla \cdot \boldsymbol{u} = 0$, we define two scalar functions, Ψ and Φ, as $\boldsymbol{B} = B_z(r,z)\boldsymbol{e}_z + \nabla\Psi \times \boldsymbol{e}_z$ and $\boldsymbol{u} = \nabla\Phi \times \boldsymbol{e}_z$. Here, $\boldsymbol{u}$ represents the perturbed velocity of the fluids, and $\boldsymbol{e}_z$ and $\boldsymbol{e}_\theta$ are the unit vectors of the longitudinal and poloidal directions of the plasma loop, respectively. We assume that the plasma density $\rho = $ const., and the resistivity $\eta = $ const., we then rewrite the magnetic induction equation and the kinetic equation as

$$\frac{\partial\Psi}{\partial t} + \boldsymbol{u}\cdot\nabla\Psi - \frac{\eta}{\mu_0}\bigtriangledown^2\,\Psi = B_z\frac{\partial\Phi}{\partial z} - \frac{\eta}{\mu_0}\frac{\partial B_z}{\partial z}, \quad (2)$$

and

$$\rho\,\frac{d}{dt}\left(\bigtriangledown^2\Phi\right) + \frac{1}{\mu_0}\,\boldsymbol{e}_z\cdot\left[\nabla\Psi\times\nabla\left(\bigtriangledown^2\Psi\right)\right] = \rho\,\frac{d}{dt}\left(\frac{\partial^2\Phi}{\partial z^2}\right). \quad (3)$$

The electric current density is $j_z \simeq -(1/\mu_0)\,\bigtriangledown^2\,\Psi$. The right-hand side in equations (2) and (3) reflect the longitudinal nonuniformity in the flare loops. For a linear perturbation, we assume its form as

$$P_1 = P\exp[i(\boldsymbol{k}\cdot\boldsymbol{l} + \omega t)] = P\exp\left[i\left(m\theta - \frac{n}{R_0}z + \omega t\right)\right], \quad (4)$$

where ω is the temporal factor that reflects the growth rate and pulsations of the tearing-mode instability in the plasma loops. $\boldsymbol{l}$ is the perturbed displacement of the fluids, and $\boldsymbol{u} = d\boldsymbol{l}/dt$, n and m are the longitudinal and poloidal mode numbers, respectively. When we linearize equations (2) and (3) we obtain the equation for the temporal factor ω,

$$\omega^2 - i\frac{\eta k^2}{\mu_0}\omega + \frac{rB_{z0}}{R_0\rho m}\left(n - \frac{m}{q}\right)\left(\frac{\partial j_z}{\partial r} + \frac{k^2}{\mu_0}B_\theta\right) = 0. \quad (5)$$

It is necessary to normalize the above equation with a series of normalized parameters for convenience. Here we define several normalized parameters: $r = ax$, $\omega = (2\pi/t_r)f$, $t = t_r\tau$, $B_\theta = B_{\theta a}B, j_z = (B_{\theta a}/\mu_0 a)j, t_r = \mu_0 a^2/\eta, t_{A\theta} = a/v_{A\theta}, S = t_r/t_{A\theta}$,

$v_{A\theta} = B_{\theta a}(\rho\mu_0)^{-1/2}$, $B_{\theta a} = \mu_0 I/2\pi a$, $k^2 = n^2/R_0^2 + m^2/r^2 = a^{-2}(n^2\epsilon^2 + m^2/x^2)$, $\epsilon = a/R_0$, $b = B_{\theta a}/B_{z0}$, and $q_0 = aB_{z0}/R_0B_{\theta a} = \epsilon/b$. Here, a is the section radius of the flare loop, R_0 is the main radius of the loop, and I is the total electric current. Then we obtain the normalized expression of the temporal factor equation

$$f^2 - i\frac{n^2\epsilon^2 + (m^2/x^2)}{2\pi}f - \frac{S^2\epsilon x}{4\pi^2 bm} \times \left(\frac{mB}{q_0 x} - n\right)\left[\left(n^2\epsilon^2 + \frac{m^2}{x^2}\right)B + \frac{\partial j}{\partial x}\right] = 0. \quad (6)$$

Its solution is

$$f = \frac{n^2\epsilon^2 + m^2/x^2}{4\pi}i \pm \frac{S}{2\pi}\sqrt{M}. \quad (7)$$

Here,

$$M = \frac{\epsilon x}{bm}\left(\frac{mB}{q_0 x} - n\right)\left[\left(n^2\epsilon^2 + \frac{m^2}{x^2}\right)B + \frac{\partial j}{\partial x}\right] - \frac{\left(n^2\epsilon^2 + m^2/x^2\right)^2}{4S^2}.$$

When $M > 0$, the above solution is made up of two parts: the imaginary part (f_i) reflects the growth rate of the linear tearing mode, and the real part (f_r) reflects the oscillations of the linear process of the tearing-mode instability. Generally, in flare loops $S \gg 10^{10}$, the second part in M may be neglected. Then the normalized growth rate's, f_i and f_r, oscillating frequency may be expressed as

$$f_i(x) = \frac{n^2\epsilon^2 + (m^2/x^2)}{4\pi}, \quad (8)$$

and

$$f_r(x) = \frac{S}{2\pi}\sqrt{M(x)}. \quad (9)$$

From equation (6) or (7), we can find that, when the relation $q_0 x/B = m/n$ is satisfied, f_i reaches to its maximum, $f_{i\,\max} = [n^2\epsilon^2 + (m^2/x^2)]/2\pi$. When we substitute the normalized parameters into f_i we obtain the maximal growth rate of the resistive tearing modes, $\omega_{i\,\max} = [n^2\epsilon^2 + (m^2/x^2)]/t_r$. The place where the above relation is satisfied may be referred to the rational surface (r_s). When the relation $M \leq 0$ is satisfied, we define a half-width δ so that the region between $r_s - \delta$ and $r_s + \delta$ is called the inner region of the tearing-mode instability. It is obvious that the resistivity plays a key role in the growth rate of the tearing-mode instability.

Based on equation (9), we obtain the period (P) of oscillations by substituting the normalized parameters into the real part of the above solution,

$$P(x) = \frac{2\pi}{\omega_r} = \frac{2\pi}{(2\pi/t_r)f_r} = \frac{2\pi t_{A\theta}}{\sqrt{M(x)}}. \quad (10)$$

From the above solution, we find that the period of the oscillations mainly depends on several factors:

1. For the total electric current (I), $P \propto 1/I$. This result is consistent with Zaitsev's model (Zaitsev et al. 1998).

2. For the geometrical parameters of the loop, a and R_0, the loop section radius a is especially sensitive to the period of the pulsations, $P \propto a^2$.

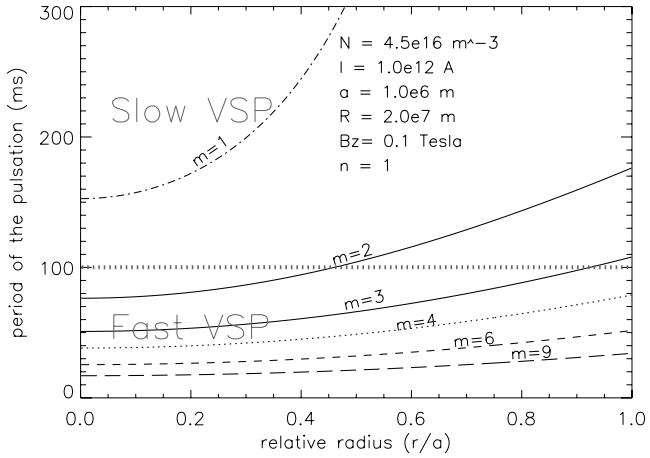

FIG. 6.—Pulsation period due to the tearing-mode oscillation with different poloidal mode numbers in the flare loops. The fast VSP is located below the broad dashed line at 100 ms, where the poloidal number is $m > 2$, and the slow VSP is located above the broad dashed line, where $m \leq 2$.

3. For the plasma density ρ, $P \propto \sqrt{\rho}$; here, $\rho = N_e m_e + N_i m_i \approx N_e m_i$.

4. The distribution of the current density in the section of the flare loops dominates the poloidal magnetic field and the value of $M(x)$.

When the loop's parameters (a, R_o, I, ρ, and T_e) are fixed, the distribution of the current density [$j_z(r)$] will become the main determinant of the pulsation period of the resistive tearing modes. For example, suppose that the current density distribution is satisfied to the pinch model (Bennett 1934; Tan 2007): $j_z(r) = (2I/\pi)\left[a^2/(a^2 + r^2)^2\right]$. Then we obtain the distribution of the pulsation period in the plasma loops (Fig. 6).

In our observation for the pulsating events, the frequency is at 2.60–3.80 GHz, and the corresponding plasma density is about 10^{16}–10^{17} m^{-3}. Thus, in our calculation, we assume the plasma density is $N_e = 4.5 \times 10^{16}$ m^{-3}, the total electric current of the loop is $I = 1.0 \times 10^{12}$A, the section radius is $a = 1.0 \times 10^6$ m, the loop main radius is $R_0 = 2.0 \times 10^7$ m, and the longitudinal magnetic field is $B_{z0} = 0.1$ T; then $b \sim 2$ and $\epsilon \sim 0.05$. For simplicity, we let the mode number be $n = 1$. Generally, such parameters are consistent with the observations of the flare loops (Bray et al. 1991). From Figure 6 we find that the shorter the period of the oscillation, the greater the poloidal number m. When $m = 1$, the pulsation period of the tearing modes is $P \geq 152$ ms, and it belongs to the slow VSP. When $m = 2$, $P = 77$–176 ms; when $m = 3$, $P = 50$–108 ms; when $m = 4$, $P = 39$–79 ms, etc. They are coincident with the periods of the fast VSPs of microwave emissions mentioned in § 2. In Figure 6 the region below the broad dashed line is the oscillation for fast VSPs, $m > 2$, and above the broad dashed line, for slow VSPs, $m \leq 2$. So, it is reasonable to propose that the pulsations of the microwave emission are the result of the modulation of the resistive tearing-mode oscillation in the current-carrying flare loops.

4. DISCUSSIONS AND CONCLUSIONS

From Figures 1, 2, 5, and Table 1, we find that the microwave pulsating events are related to various type of bursts. Their background may be of the type IV bursts, type III bursts, zebra patterns, and even spikes. Then we can assume that the pulsating events might be the result of microwave emissions modulated by some oscillators. As the periods of the resistive tearing-mode

oscillations in current-carrying flare loops are coincident with the above observation of pulsating events, it is reasonable to assume that it was the resistive tearing-mode oscillation in the current-carrying flare loops that modulated the microwave emissions and formed the pulsating structures.

From the analysis in § 3 we find that the resistive tearing modes have two-sided properties. Equation (8) indicates the instabilities of the resistive tearing modes, and equation (9) shows the property of oscillation. The evolution of the resistive tearing-mode instability dominates the processes of magnetic reconnection, particle acceleration, energy dissipation, and the emission mechanism, while the tearing-mode oscillation will modulate the microwave emission and result in the pulsating structures.

Based on the above conclusions, we suggest that the process of forming the pulsating events as:

1. The flaring region consists of many current-carrying compact loops. In our case, the X3.4 flare event occurred in a complex active region (AR 10930), so it is reasonable to work out the above assumption.

2. In each current-carrying flare loop, the resistive tearing-mode instability will trigger the formation of a series of multiscale magnetic islands (with different poloidal number m). The positions of X-points is between two magnetic islands. There are many X-points in each flare loop. In the three-dimensional space, X-points will form X-lines (separatrix; Furth et al. 1973; Biskamp & Welter 1980; Hegna & Bhattacharjee 1989; Watanabe et al. 1999).

3. Electron accelerations occur in the regions near each X-points, and the energetic electrons are distributed mainly along the X-lines of the magnetic configuration in the current-carrying flare loops. The motion of the energetic electrons will form a particle beam. As there are many X-points in each flare loop, there are simultaneously a great number of energetic particle beams. Such an electron acceleration process is a bit similar to the stochastic particle acceleration model (Vlahos et al. 2004). During these processes, the plasma emission is generated (Karlický & Bárta 2007). If there were no modulators, the emission would behave as a continuum.

4. However, the resistive tearing-mode oscillation will modulate the above plasma emission, turning the emission spectrogram into pulsating structures. The evolution of the tearing-mode instability dominates the duration of the pulsating events, and the period of the tearing-mode oscillation governs the period of the pulsating events.

5. The motion of the energetic electron beam forming from the region near the X-points causes the plasma emissions to have a frequency drift, which is seen as the frequency drifting rate in each single pulse (SPFDR). As usual, the velocity of the energetic electron beam is very high, so the frequency drifting rate is very large. The moving direction of the energetic electron beam is from the accelerated region (X-points) to the inner part of the magnetic island (plasmoid), the plasma density gradient is always positive (Karlický & Bárta 2007), and this results in a SPFDR > 0 at all times. The range of the plasma density from the X-point to the inner part of the magnetic islands governs the emission frequency and consequently implicates the bandwidth of the emission. According to the result of Karlický & Bárta (2007), the range is about $0.83n_0$–$8.3n_0$, where n_0 is the density apart from the rational surface. Thus, the pulsating events are related with broad bandwidth emission.

6. The motion of the flare loop causes the global frequency drifting rate (GFDR). When the motion is from the lower to the higher corona, the plasma density gradient is negative, and GFDR < 0. When the motion of the flare loop is from the higher to the lower corona (shrinkage of the flare loop; Li & Gan 2005; Vrsnak et al. 2006), the plasma density gradient is positive, GFDR > 0, and when the flare loop is at rest, GFDR $\rightarrow 0$.

The above results indicate that the microwave pulsations are the signatures of the electromagnetic structure in the solar flaring regions. From equation (10) and the definition of $t_{A\theta}$, we find that the periods of the tearing-mode oscillations are sensitive to the section radius (a^2), the total current (I^{-1}), and the plasma density ($\rho^{1/2}$). In the mean time, the gradient of the current density $\partial j_z/\partial r$ also plays an important role in the periods of the tearing-mode oscillations. If we obtain microwave spectrograms with high cadence and a high resolution of the frequency, in addition to radioheliographs with high resolution in space instantaneously, then we can distinguish the detailed electromagnetic structure of the flaring region, and this will help us to understand the physical mechanism of the eruptive processes.

The authors would like to thank the helpful and useful suggestions and discussions with M. Karlický, Q. J. Fu, and G. L. Huang. This work was supported by the National Basic Research Program of the MOST (grant 2006CB806301), NSFC grant 10333030, and CAS-NSFC Key Project (grant 10778605).

REFERENCES

Aschwanden, M. J. 1987, Sol. Phys., 111, 113
———. 2004, Physics of the Solar Corona: An Introduction (Berlin: Springer)
Bennett, W. H. 1934, Phys. Rev., 45, 90
Biskamp, D., & Welter, H. 1980, Phys. Rev. Lett., 44, 1069
Bray, R. J., Cram, L., Durrant, C. J., & Loughhead, R. E. 1991, Plasma Loops in the Solar Corona (Cambridge: Cambridge Univ. Press)
Chiu, Y. T. 1970, Sol. Phys., 13, 420
Drake, J. F., Swisdak, M., Che, H., & Shay, M. A. 2006, Nature, 443, 553
Elgarøy, E. 1986, Sol. Phys., 104, 43
Fu, Q. J., Gong, Y. F., Jin, S. Z., & Zhao, R. Y. 1990, Sol. Phys., 130, 161
Fu, Q. J., Qin, Z., Ji, H., & Pei, L. 1995, Sol. Phys., 160, 97
Fu, Q. J., et al. 2004, Sol. Phys., 222, 167
Furth, H. P., Rutherford, P. H., & Selberg, H. 1973, Phys. Fluids, 16 , 1054
Gotwols, B. L. 1972, Sol. Phys., 25, 232
Hassam, A. B. 1990, ApJ, 348, 778
Hegna, C. C., & Bhattacharjee, A. 1989, Phys. Fluids B, 1, 392
Heyvaerts, J., Priest, E. R., & Rust, D. 1977, ApJ, 216, 123
Huang, G. L. 1990, Adv. Space Res., 10, 173
Karlický, M. 2004, A&A, 417, 325
Karlický, M., & Bárta, M. 2007, A&A, 464, 735
Karlický, M., Bárta, M., Mészárová, H., & Zlobec, P. 2005, A&A, 432, 705
Karlický, M., & Odstrćil, D. 1994, Sol. Phys., 155, 171
Khan, J. I., Vilmer, N., Saint-Hilaire, P., & Benz, A. O. 2002, A&A, 388, 363
Khodachenko, M. L., & Rucker, H. O. 2005, Adv. Space Res., 36, 1561
Kliem, B., Karlicky, M., & Benz, A. Q. 2000, A&A, 360 , 715
Kundu, M. R., Nindos, A., Vilmer, N., Klein, K.-L., Shibata, K., & Ohyama, M. 2001, ApJ, 559, 443
Li, Y. P., & Gan, W. Q. 2005, ApJ, 629, L137
Ma, Y., Xie, R. X., Zhang, X. M., & Huang, G. L. 2003, Sol. Phys., 214, 353
Nakariakov, V. M., Melnikov, V. F., & Reznikova, V. E. 2003, A&A, 412, L7
Spicer, D. S. 1981, Sol. Phys., 71, 115
Tan, B. L. 2007, Adv. Space Res., 39, 1825
Tan, B. L., & Huang, G. L. 2006, A&A, 453, 321
Tan, B. L., Ji, H. S., Huang, G. L., Zhou, T. H., Song, Q. W., & Huang, Y. 2006, Sol. Phys., 239, 137
Thompson, A. R., & Maxwell, A. 1962, ApJ, 136, 546

Vlahos, L., Isliker, H., & Lepreti, F. 2004, ApJ, 608, 540
Vrsnak, B., Temmer, M, Veronig, A., Karlicky, M., & Lin, J. 2006, Sol. Phys., 234, 273
Wang, M., & Xie, R. X. 2000, Chin. J. Astron. Astrophys., 24, 95
Watanabe, T.-H., Hayashi, T., & Sato, T. 1999, Phys. Plasma, 6, 1253
Yan, Y. H., Huang, J., Chen, B., & Sakurai, T. 2007, PASJ, in press
Yan, Y. H., Tan, C. M., Xu, L., Ji, H. R., Fu, Q. J., & Song, G. X. 2002, Science in China Ser. A, 45, 89 (Supplement)
Young, C. W., Spencer, C. L., & Moreton, G. E. 1961, ApJ, 133, 243
Zaitsev, V. V., Stepanov, A. V., & Sterlin, A. M. 1985, Sov. Astron. Lett., 11, 192
Zaitsev, V. V., Stepanov, A. V., Urpo, S., & Pohjolainen, S. 1998, A&A, 337, 887